

Quantitative metallography of deformed grains

Q. Zhu¹, C. M. Sellars² and H. K. D. H. Bhadeshia^{*3}

The effect of plastic deformation on the grain boundary surface area per unit volume and edge length per unit volume is examined using two methods. The first by applying homogeneous deformations to tetrakaidecahedra in a variety of orientations and the second by using the principles of stereology. It is shown that the methods produce essentially identical results. It is now possible to calculate changes in the grain parameters as a function of a variety of deformations, for combinations of deformations, for complex deformations and for cases where it is not necessary to assume an idealised grain microstructure.

Keywords: Stereology, Quantitative metallography, Deformation, Tetrakaidecahedron

Introduction

Steels and aluminium alloys are produced in very large quantities using plastic deformation in order to achieve particular shapes of use in industry. The microstructure changes during deformation, with an increase in the defect density and in the amount of grain boundary area per unit volume S_V and grain edge length per unit volume L_V . All of these changes are important in determining the course of phase transformations in steels and recrystallisation processes in general.

The evolution of grain shape and its influence on S_V and L_V were first considered by Underwood using stereological methods.¹ These assumed that grains are space filling and equiaxed, but did not require them to have a specific initial shape. Underwood considered three types of deformation common in metalworking processes:

- (i) plane strain compression, which was called 'planar-linear orientation', typical in flat product rolling
- (ii) axisymmetric compression, which was called 'planar orientation', typical of upset forging
- (iii) axisymmetric tensile deformation, which was called 'linear orientation', typical for long product rolling, wire drawing and extrusion.

The principal strain components were considered to be homogeneous and no analysis was given of the effects of redundant shear strains, which always arise and vary through the cross-section owing to surface friction effects in all real metalworking processes.

The evolution of grain shape has also been studied analytically²⁻⁶ and experimentally.⁷ Umemoto *et al.*⁸

first estimated the change in S_V as a function of strain by representing the undeformed grains as spheres. Recently, Bate and Hutchinson⁹ have used the same assumption to compute S_V for the strain systems considered by Underwood, and for simple shear. Additionally, they use a crystal plasticity finite element model to compute the effects of non-uniform deformation of grains, arising from the constraints of neighbouring grains of different crystallographic orientation. Since spheres are not space filling and do not have edges, other researchers have represented the initial grain shapes as cubes¹⁰⁻¹² or as Kelvin tetrakaidecahedra^{1,4} to represent the undeformed grain. Cubes simplify the mathematical analysis, but clearly are poor approximations to the shapes of real grains, whereas tetrakaidecahedra give sections which approximate closely to grain shapes observed metallographically. They also have angles between grain faces, which nearly satisfy equilibrium of interfacial tensions, requiring only minor boundary curvatures to balance the tensions at grain boundary junctions.

A tetrakaidecahedron has eight hexagonal and six square faces, Fig. 1, with 36 edges, each of length a . All of the edges can be described in terms of just six vectors, as listed in Table 1. In previous work,⁴ the axes of the deformation matrix were defined as illustrated in Fig. 1; in other words, the orientation of the grain was chosen in order to conveniently derive the deformation equations. This may be a weakness since in a real material the edges of the grains are likely to be randomly oriented relative to the principal axes of the deformation. The purpose of the present work is to address these issues and to generalise the calculations to a greater variety of industrially important deformations, including redundant shear strains.

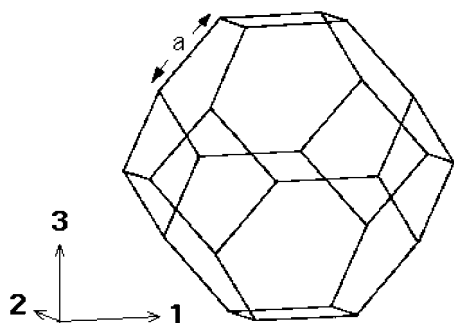
Throughout the present work, it is assumed that the deformation is homogeneous; the potential effects of shear bands or mechanical twinning are not dealt with, nor is the creation of new high misorientation boundaries by grain subdivision or by annealing twins losing coherency during deformation.

¹Holset Engineering Co. Ltd, St Andrew's Road, Huddersfield HD1 6RA, UK

²Institute of Microstructural and Mechanical Processing, The University of Sheffield (IMMPETUS), Mappin Street, Sheffield S1 3JD, UK

³Department of Materials Science and Metallurgy, University of Cambridge, Pembroke Street, Cambridge CB2 3QZ, UK

*Corresponding author, email hkdb@cam.ac.uk



1 Tetrakaidecahedron

Analysis method

Plane strain deformation

A general deformation matrix S acts on a vector u to give a new vector v as follows^{3,4,13}

$$\begin{pmatrix} S_{11} & S_{12} & S_{13} \\ S_{21} & S_{22} & S_{23} \\ S_{31} & S_{32} & S_{33} \end{pmatrix} \begin{pmatrix} u_1 \\ u_2 \\ u_3 \end{pmatrix} = \begin{pmatrix} v_1 \\ v_2 \\ v_3 \end{pmatrix} \quad (1)$$

Consider first the orientation of the tetrakaidecahedron as illustrated in Fig. 1. The tetrakaidecahedron is completely specified by the six initial vectors listed in Table 1. For plane strain deformation, all S_{ij} in equation (1) are zero except that $S_{11} \times S_{22} \times S_{33} = 1$ to conserve volume and $S_{11} \times S_{33} = 1$ since $S_{22} = 1$. For a diagonal matrix, the terms S_{11} , S_{22} and S_{33} represent the principal distortions, i.e. the ratios of the final to initial lengths of unit vectors along the principal axes. It follows that for a diagonal S , the true strains are given by $\epsilon_{11} = \ln(S_{11})$, $\epsilon_{22} = \ln(S_{22})$ and $\epsilon_{33} = \ln(S_{33})$.

The application of the deformation to the initial set of vectors results in the new set of vectors listed in Table 2. The latter are used to calculate the area and edge lengths of the deformed object. Using equation (1) and the conditions for plane strain deformation, it can be shown that the final to initial area (A/A_0) and edge-length (L/L_0) ratios for the deformed tetrakaidecahedron are given by

$$\frac{A}{A_0} \equiv \frac{S_V}{S_{V_0}} = \frac{S_{11} + 3[S_{11}(1 + 2S_{33}^2)^{1/2} + (S_{11}^2 + 2S_{33}^2)^{1/2}] + S_{33}[2(1 + S_{11}^2)]^{1/2}}{3(2\sqrt{3} + 1)} \quad (2)$$

$$\frac{L}{L_0} \equiv \frac{L_V}{L_{V_0}} = \frac{1 + S_{11} + 2(1 + S_{11}^2 + 2S_{33}^2)^{1/2}}{6} \quad (3)$$

where S_{V_0} and L_{V_0} are the values at zero strain, of grain surface area and edge length per unit volume. These

Table 1 Vectors defining edges of tetrakaidecahedron

Vector	Components
1	$[a \ 0 \ 0]$
2	$[0 \ a \ 0]$
3	$[-\frac{a}{2} \ -\frac{a}{2} \ \frac{a}{\sqrt{2}}]$
4	$[\frac{a}{2} \ -\frac{a}{2} \ \frac{a}{\sqrt{2}}]$
5	$[\frac{a}{2} \ \frac{a}{2} \ \frac{a}{\sqrt{2}}]$
6	$[-\frac{a}{2} \ \frac{a}{2} \ \frac{a}{\sqrt{2}}]$

equations apply strictly to the grain orientation illustrated in Fig. 1, relative to S . From stereology,¹ $S_{V_0} = 2/\bar{L}$ so that $S_V/S_{V_0} \equiv 2S_V\bar{L}$, and $L_{V_0} = 9.088/\bar{L}^2$, where \bar{L} is the mean linear intercept commonly used to define the grain size.^{13,14} It follows that equations (2) and (3) implicitly contain the grain size as an input variable.

The grain orientation illustrated in Fig. 1 may not be representative. Suppose that it is required to orient the tetrakaidecahedron randomly with respect to the deformation. A rotation matrix R can be generated using random numbers to rotate the object relative to the axes defining S . Equation (1) then becomes

$$\begin{pmatrix} S_{11} & S_{12} & S_{13} \\ S_{21} & S_{22} & S_{23} \\ S_{31} & S_{32} & S_{33} \end{pmatrix} \begin{pmatrix} R_{11} & R_{12} & R_{13} \\ R_{21} & R_{22} & R_{23} \\ R_{31} & R_{32} & R_{33} \end{pmatrix} \begin{pmatrix} u_1 \\ u_2 \\ u_3 \end{pmatrix} = \begin{pmatrix} v_1 \\ v_2 \\ v_3 \end{pmatrix} \quad (4)$$

The results are illustrated in Fig. 2. For comparison, the results are plotted against the equivalent strain

$$\epsilon = \left(\frac{2}{3}\right)^{1/2} \left(\epsilon_{11}^2 + \epsilon_{22}^2 + \epsilon_{33}^2 + \frac{1}{2}\gamma_{13}^2 + \frac{1}{2}\gamma_{12}^2 + \frac{1}{2}\gamma_{23}^2\right)^{1/2} \quad (5)$$

where ϵ_{11} , ϵ_{22} and ϵ_{33} are the normal components and γ_{13} , γ_{12} and γ_{23} are the shear components of strain (the tangents of the shear angles). For homogeneous plane strain compression, $\epsilon = (2/\sqrt{3})\epsilon_{11}$. In Fig. 2, the dashed line represents the outcome for the orientation illustrated in Fig. 1 and the points are for the 99 other results of randomly oriented tetrakaidecahedra. It is clear that the orientation of the tetrakaidecahedron does not make much of a difference to the outcome as far as the surface and edge lengths per unit volume are concerned. This is probably because the tetrakaidecahedron is almost isotropic in shape.

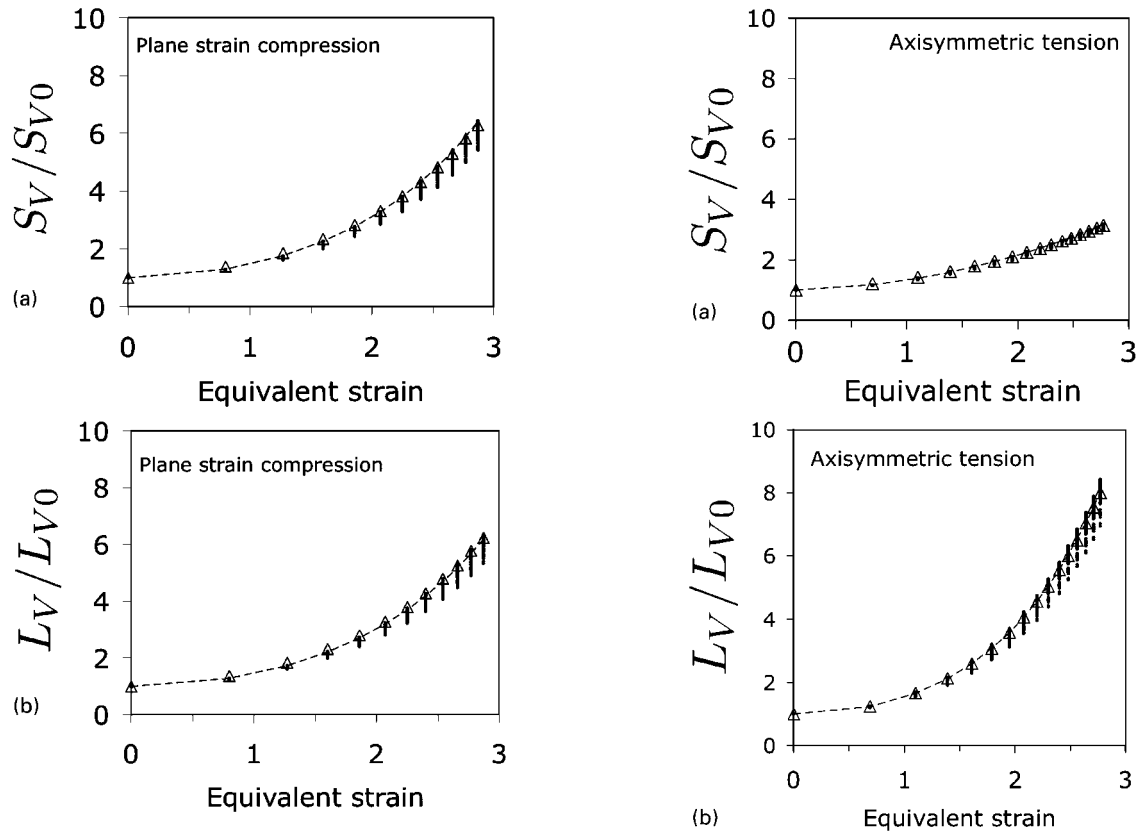
Axisymmetric tension

In wire drawing or rod rolling, $S_{22} = S_{33}$ and volume conservation requires that $S_{22} = 1/(S_{11})^{1/2}$ (Table 3). For the tetrakaidecahedron oriented as in Fig. 1

$$\frac{S_V}{S_{V_0}} = \frac{(3S_{11})^{1/2} + \left(\frac{2}{S_{11}^2} + S_{11}\right)^{1/2} + \frac{1}{3} + \frac{1}{3}\left(\frac{2}{S_{11}^2} + 2S_{11}\right)^{1/2}}{1 + 2\sqrt{3}} \quad (6)$$

Table 2 Components of six vectors listed in Table 1, after plane strain or axisymmetric deformation

Deformed vector	Components
1	$[aS_{11} \ 0 \ 0]$
2	$[0 \ aS_{22} \ 0]$
3	$[-\frac{aS_{11}}{2} \ -\frac{aS_{22}}{2} \ \frac{aS_{33}}{\sqrt{2}}]$
4	$[\frac{aS_{11}}{2} \ -\frac{aS_{22}}{2} \ \frac{aS_{33}}{\sqrt{2}}]$
5	$[\frac{aS_{11}}{2} \ \frac{aS_{22}}{2} \ \frac{aS_{33}}{\sqrt{2}}]$
6	$[-\frac{aS_{11}}{2} \ \frac{aS_{22}}{2} \ \frac{aS_{33}}{\sqrt{2}}]$



a area ratio versus equivalent strain; b edge ratio versus equivalent strain

2 Calculations for plane strain deformation: curve represents data for tetrakaidecahedron oriented as illustrated in Fig. 1; small points are 99 other cases where tetrakaidecahedron is randomly oriented relative to S; triangular points for area ratio are from equation (21) and for edge ratio from equation (26) as discussed later

$$\frac{L_V}{L_{V_0}} = \frac{S_{11} + S_{11}^{-1} + 2(S_{11}^2 + 3S_{11}^{-1})^{1/2}}{6} \quad (7)$$

The results are illustrated in Fig. 3, where it is particularly noticeable that the increase in edge length relative to grain boundary area, as a function of strain, is exaggerated when compared with the corresponding case for plane strain compression.

Axisymmetric compression

In axisymmetric compression, $S_{11} = S_{22} = 1/(S_{33})^{1/2}$, and for a tetrakaidecahedron oriented as in Fig. 1

$$\frac{S_V}{S_{V_0}} = \frac{\left[8S_{33} + \frac{4}{S_{33}^2}\right]^{1/2} + \frac{1}{3}\left[\frac{1}{S_{33}} + 2S_{33}^{1/2}\right]}{1 + 2\sqrt{3}} \quad (8)$$

$$\frac{L_V}{L_{V_0}} = \frac{1}{3} \left[(S_{33})^{1/2} + \left(2S_{33}^2 + \frac{2}{S_{33}}\right)^{1/2} \right] \quad (9)$$

The results are illustrated in Fig. 4.

Table 3 Volume preserving deformations*

Type	S_{11}	S_{12}	S_{13}	S_{21}	S_{22}	S_{23}	S_{31}	S_{32}	S_{33}
Plane strain compression	≥ 1	0	0	0	1	0	0	0	$1/S_{11}$
Axisymmetric compression	$1/(S_{33})^{1/2}$	0	0	0	$1/(S_{33})^{1/2}$	0	0	0	≤ 1
Axisymmetric tension	≥ 1	0	0	0	$1/(S_{11})^{1/2}$	0	0	0	$1/(S_{11})^{1/2}$
Simple shear	1	0	+ve	0	1	0	0	0	1

*The convention used is that $S_{11} > S_{22} > S_{33}$.

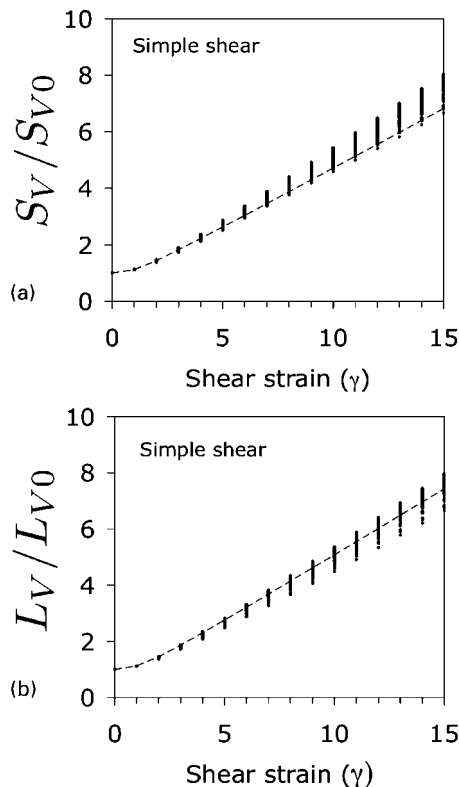
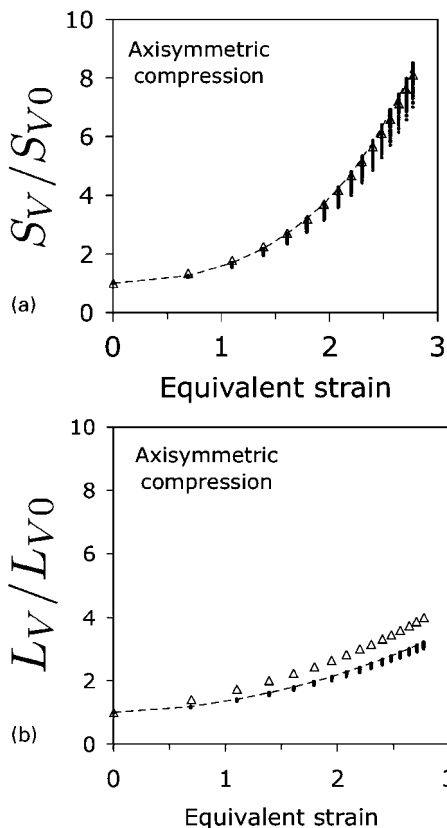
a area ratio versus equivalent strain; b edge ratio versus equivalent strain

3 Calculations for axisymmetric tension: curve represents data for tetrakaidecahedron oriented as illustrated in Fig. 1; small points are 99 other cases where tetrakaidecahedron is randomly oriented relative to S; triangular points for area ratio are from equation (21) and for edge ratio from equation (27) as discussed later

Simple shear

Torsion testing, which involves shear deformation, is often used to determine the constitutive equations for austenite. During shear deformation, $S_{11} = S_{22} = S_{33} = 1$, S_{13} is the shear strain, and all the other elements of S are zero (Table 3). On substituting these boundary conditions and the undeformed vectors into equation (1), the deformed vector components listed in Table 4 are obtained. The resulting analytical equations defining the deformation of the tetrakaidecahedron oriented as illustrated in Fig. 1 are found to be

$$\frac{S_V}{S_{V_0}} = \frac{2 + 4\left(1 + \frac{S_{13}^2}{4}\right)^{1/2} + 12\sqrt{\frac{3}{4}}}{6(1 + 2\sqrt{3})} + \frac{6\left(\frac{3}{4} + \frac{S_{13}^2}{2} + \frac{S_{13}}{\sqrt{2}}\right)^{1/2} + 2\left[\left(3 + 2S_{13}^2 - \frac{4S_{13}}{\sqrt{2}}\right)^{1/2} + \left(\frac{3}{4} + \frac{S_{13}^2}{2} - \frac{S_{13}}{\sqrt{2}}\right)^{1/2}\right]}{6(1 + 2\sqrt{3})} \quad (10)$$



a area ratio versus equivalent strain; b edge ratio versus equivalent strain

4 Calculations for axisymmetric compression: curve represents data for tetrakaidecahedron oriented as illustrated in Fig. 1; small points are 99 other cases where tetrakaidecahedron is randomly oriented relative to S; triangular points are based on equation (21) for area ratio and equation (28) for edge ratios

$$\frac{L_V}{L_{V_0}} = \frac{1}{3} \left[1 + \left(1 + \frac{S_{13}^2}{2} - \frac{S_{13}}{\sqrt{2}} \right)^{1/2} + \left(1 + \frac{S_{13}^2}{2} + \frac{S_{13}}{\sqrt{2}} \right)^{1/2} \right] \quad (11)$$

The general results for shear are illustrated in Fig. 5, with the horizontal axes both plotted in terms of shear strain.

Sequential deformations

The method here is general – all that is needed is to define the matrix S for the appropriate

Table 4 Components of six vectors listed in Table 1 after shear deformation

Deformed vector	Components
1	[a 0 0]
2	[0 a 0]
3	$\left[\frac{aS_{13}}{\sqrt{2}} - \frac{a}{2} - \frac{a}{2} \frac{a}{\sqrt{2}} \right]$
4	$\left[\frac{aS_{13}}{\sqrt{2}} + \frac{a}{2} - \frac{a}{2} \frac{a}{\sqrt{2}} \right]$
5	$\left[\frac{aS_{13}}{\sqrt{2}} + \frac{a}{2} \frac{a}{\sqrt{2}} \right]$
6	$\left[\frac{aS_{13}}{\sqrt{2}} - \frac{a}{2} \frac{a}{\sqrt{2}} \right]$

a area ratio versus shear strain; b edge ratio versus shear strain

5 Calculations for shear deformation: curve represents data for tetrakaidecahedron oriented as illustrated in Fig. 1; small points are 99 other cases where tetrakaidecahedron is randomly oriented relative to S

circumstances. There are cases where two or more different kinds of deformation are used in sequence, for example, cross-rolling in which the plate is rotated through 90° after a degree of reduction. This is readily tackled by generalising equation (1). Rotation through 90° about the compression axis [0 0 1] is given by¹³

$$R = \begin{pmatrix} 0 & 1 & 0 \\ -1 & 0 & 0 \\ 0 & 0 & 1 \end{pmatrix} \quad (12)$$

Writing the first rolling pass as S and the cross-rolling pass as T, the net deformation U is given by TRS

$$U = \begin{pmatrix} T_{11} & 0 & 0 \\ 0 & 1 & 0 \\ 0 & 0 & 1/T_{11} \end{pmatrix} \begin{pmatrix} 0 & 1 & 0 \\ -1 & 0 & 0 \\ 0 & 0 & 1 \end{pmatrix} = \begin{pmatrix} 0 & T_{11} & 0 \\ -S_{11} & 0 & 0 \\ 0 & 0 & \frac{1}{T_{11}S_{11}} \end{pmatrix} \quad (13)$$

Complex deformations

Flat product rolling is approximated as plane strain compression, but friction with the rolls leads to shears. The plane strain condition is strictly

satisfied only at the centre of the rolled material. The matrix S can be used to deal with the simultaneous actions of plane strain compression and simple shear (on the rolling plane and in the rolling direction) by generalising the deformation matrix equation (1) as follows

$$\begin{pmatrix} S_{11} & 0 & S'_{13} \\ 0 & 1 & 0 \\ 0 & 0 & 1/S_{11} \end{pmatrix} \quad (14)$$

The final shear strain S'_{13} arises from the imposed shear strain S_{13} , modified by the compression S_{11} and is represented by $S_{13} \times S_{11}$.

Metrology

As pointed out in the introduction, real microstructures will contain a distribution of grain sizes. This is enshrined on a statistical basis in stereological parameters such as the mean linear intercept \bar{L} , etc. It is useful therefore to see whether the outcomes discussed in the previous sections can be reproduced using stereology.

The volume, surface area and edge length of an undeformed tetrakaidecahedron (Fig. 1) are given by

$$V_0 = 8\sqrt{2}a^3 \quad S_0 = 6(1 + 2\sqrt{3})a^2 \quad \text{and} \quad L_0 = 36a \quad (15)$$

It follows that for a uniform grain structure

$$S_{V_0} = \frac{3(1 + 2\sqrt{3})}{8\sqrt{2}a} \quad \text{and} \quad L_{V_0} = \frac{3}{2\sqrt{2}a^2} \quad (16)$$

The mean linear intercept representing the undeformed grain size measured on two-dimensional sections therefore becomes

$$\bar{L}_0 = \frac{2}{S_{V_0}} = \frac{16\sqrt{2}a}{3(1 + 2\sqrt{3})} \quad (17)$$

For a deformed grain, given that the number of boundaries per unit length $N_{L1} \leq N_{L2} \leq N_{L3}$, the surface per unit volume from Ref. 1 is

$$S_V = 0.429N_{L1} + 0.571N_{L2} + N_{L3} \quad (18)$$

and since $\bar{L} = 1/N$, for plastic deformation in which $\epsilon_{11} \geq \epsilon_{22} \geq \epsilon_{33}$, the linear intercepts are

$$\begin{aligned} \bar{L}_1 &= \bar{L}_0 \exp\{\epsilon_{11}\} & \bar{L}_2 &= \bar{L}_0 \exp\{\epsilon_{22}\} \\ \bar{L}_3 &= \bar{L}_0 \exp\{\epsilon_{33}\} \end{aligned} \quad (19)$$

so that

$$S_V = \bar{L}_0^{-1} (0.429 \exp\{-\epsilon_{11}\} + 0.571 \exp\{-\epsilon_{22}\} + \exp\{-\epsilon_{33}\}) \quad (20)$$

$$\begin{aligned} \frac{S_V}{S_{V_0}} &= \frac{1}{2} (0.429 \exp\{-\epsilon_{11}\} + 0.571 \exp\{-\epsilon_{22}\} + \\ &\exp\{-\epsilon_{33}\}) \end{aligned} \quad (21)$$

This equation can be used in association with the boundary conditions outlined in Table 5 to estimate S_V for a variety of deformations. In Figs. 2a, 3a and 4a, the triangular points are calculated using equation (21).

When dealing with oriented structures, lines in a given volume can be categorised into segments which are

aligned parallel to one or more directions, with the remainder being randomly oriented.¹ For the anisotropic grains which result from plane strain compression (planar-linear oriented structure¹), the edge length per unit volume is the sum of three contributions from isometric (randomly oriented), planar (compressed) and linear elements (elongated) components¹

$$L_V = L_{V_{\text{isometric}}} + L_{V_{\text{planar}}} + L_{V_{\text{linear}}} \quad (22)$$

For an undeformed tetrakaidecahedron, the relationship between the edge length per unit volume and the number of points of intersections of edges with a test plane of unit area is simple, $L_V = 2P_A$.¹ For a deformed grain it is necessary to specify the three contributions of equation (22). If '1' and '3' are the rolling and thickness directions respectively, then from Ref. 1

$$\begin{aligned} L_{V_{\text{isometric}}} &= 2P_{A_3} & L_{V_{\text{planar}}} &= (P_{A_1} - P_{A_3}) \\ L_{V_{\text{linear}}} &= \frac{1}{2}(P_{A_2} - P_{A_3}) \end{aligned} \quad (23)$$

where P_{A_3} refers to the points per unit area on the plane normal to the 3-axis, etc. It follows that

$$L_V = P_{A_3} + \frac{1}{2}(P_{A_1} + P_{A_2}) \quad (24)$$

with

$$\begin{aligned} P_{A_1} &= P_A \exp\{-(\epsilon_{22} + \epsilon_{33})\} \\ P_{A_2} &= P_A \exp\{-(\epsilon_{11} + \epsilon_{33})\} \\ P_{A_3} &= P_A \exp\{-(\epsilon_{11} + \epsilon_{22})\} \end{aligned} \quad (25)$$

By combining these equations the authors obtain for plane strain deformation

$$\frac{L_V}{L_{V_0}} = \frac{1}{4} \exp\{-\epsilon_{11}\} + \frac{1}{4} \exp\{-\epsilon_{22}\} + \frac{1}{2} \exp\{-\epsilon_{33}\} \quad (26)$$

The results obtained using this equation are plotted as triangular points on Fig. 2b, showing good agreement with the data from equation (3).

Axisymmetric tension is described as a linearly oriented structure so the planar component in equation (22) is absent, resulting in a different equation for edge length per unit volume. Given 1 and 3 as the longitudinal and radial directions respectively, the authors have (equation (3.15)¹)

$$\begin{aligned} L_V &= P_{A_1} + P_{A_3} \\ &= P_{A_0} [\exp\{\epsilon_{11}\} + \exp\{-\epsilon_{11}/2\}] \\ \frac{L_V}{L_{V_0}} &= \frac{1}{2} (\exp\{-2\epsilon_{33}\} + \exp\{\epsilon_{33}\}) \end{aligned} \quad (27)$$

The excellent agreement between the different methods is illustrated in Fig. 3b.

Table 5 Strains for substitution into equations (20) and (21)*

Deformation	ϵ_{11}	ϵ_{22}	ϵ_{33}
Plane strain compression	+ve	0	$-\epsilon_{11}$
Axisymmetric tension	+ve	$-\frac{1}{2}\epsilon_{11}$	$-\frac{1}{2}\epsilon_{11}$
Axisymmetric compression	$-\frac{1}{2}\epsilon_{33}$	$-\frac{1}{2}\epsilon_{33}$	-ve

*Note that $\epsilon_{11} + \epsilon_{22} + \epsilon_{33}$ must equal zero to conserve volume, and it is assumed that $\epsilon_{11} \geq \epsilon_{22} \geq \epsilon_{33}$.

Axisymmetric compression effectively flattens the grains normal to the compression axis and hence leads to what Underwood calls a planar oriented structure (Fig. 3.13,¹). The values of P_A in the planes containing the compression axis grow rapidly whereas they decline rapidly in those normal to the compression axis. This is difficult to treat, because the degree of orientation (Ω in Underwood's terminology¹) becomes negative. This is not the case for axisymmetric tension. However, if it is assumed as an approximation that the planes containing the compression axis dominate, then

$$\frac{L_V}{L_{V_0}} \simeq \exp\{-(\varepsilon_{22} + \varepsilon_{33})\} \quad (28)$$

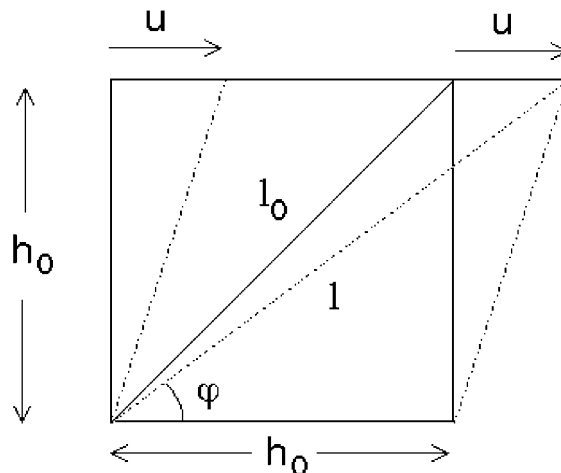
The results of these calculations are illustrated as triangular points in Fig. 4 and unusually compared with other deformation conditions, they lie above the maximum value for the tetrakaidehedra because of the approximation in equation (28).

Discussion

Deformation mode

In order to determine the flow stress and dislocation structures relevant for industrial hot working conditions, tension, axisymmetric compression, plane strain compression and torsion tests are used by different research groups. It is generally considered that the results from the different tests are consistent when they are compared at the same equivalent strain for tests at the same equivalent strain rate and temperature. The dislocation structures provide the driving force for nucleation and growth of recrystallised grains formed either dynamically or statically. In both cases nucleation occurs preferentially at grain boundaries, with grain edges being important at low strains, but grain surfaces being more important over most of the range of strains of interest in industrial hot working operations.¹⁵ Comparing the effects of equivalent strain on S_V/S_{V_0} and L_V/L_{V_0} for plane strain compression, axisymmetric tension and axisymmetric compression in Figs. 2–4, it can be seen that the maximum values for tetrakaidehedra correspond closely with the results from the metallography analysis. The values of S_V/S_{V_0} also correspond closely with the results for the deformation of spheres computed by Bate and Hutchinson,⁹ who showed that their analysis always gave higher values than analyses for the deformation of cubes.^{10–12} In this context, it is of interest to note that the minimum values from the present analysis of tetrakaidehedra are also always above the values for cubes. In further discussion, only the maximum values given by equations 2, 3 and 6–9 will be considered.

The present results for S_V/S_{V_0} and L_V/L_{V_0} in axisymmetric tension (long product rolling, wire drawing and extrusion) (Fig. 3) and in axisymmetric compression (upset forging) (Fig. 4) are antisymmetric, so tension is much less effective than compression in increasing S_V/S_{V_0} and vice versa for increasing L_V/L_{V_0} . Also, axisymmetric compression is more effective in increasing S_V/S_{V_0} than plane strain compression (flat product rolling) (Fig. 2). This difference arises mainly from the influence of the different constraints on the values of equivalent strain for a given reduction in height (ε_{33}).



6 Simple shear

For simple shear, the results in Fig. 5 are plotted against the shear strain ($\gamma = S_{13}$), because there is some controversy about how shear strains should be converted to equivalent strains. Equation (5) leading to $\varepsilon = \gamma/\sqrt{3}$ is valid for small strains, and Canova *et al.*¹⁶ argued that it is also valid for large strains. This view is frequently adopted for analysis of the results from torsion tests and from the effects of redundant shear strains in rolling and extrusion. However, Bate and Hutchinson⁹ derived a relationship for the equivalent strain from the initial and final states after simple shear deformation of spheres as follows

$$\varepsilon = \frac{2}{\sqrt{3}} \ln \left\{ \left[\frac{\gamma}{2} + \left(1 + \frac{\gamma^2}{4} \right)^{1/2} \right] \right\} \quad (29)$$

This is identical to the equation from earlier analyses for the shear deformation of spheres^{17,18} and leads to much reduced values of ε with the increase in γ compared with equation (5). An elementary geometrical analysis of the effect of simple shear (Fig. 6) leads to the result that the tensile strain along the diagonal, which undergoes a rigid body rotation with increasing strain, is

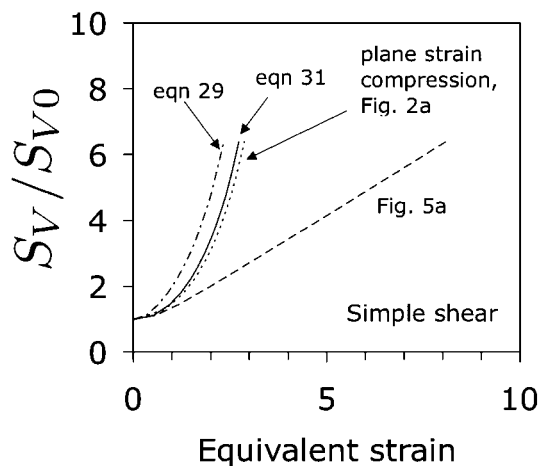
$$\varepsilon_{11} = \ln \{ \sin \phi / \sin \phi_0 \} \quad \text{and} \quad \tan \phi = (1 + \gamma)^{-1} \quad (30)$$

where $\phi = \phi_0 = 45^\circ$ when $\gamma = u/h_0 = 0$. From standard geometrical relationships and the fact that simple shear is an invariant plane strain deformation, the equivalent strain is

$$\varepsilon = \frac{2}{\sqrt{3}} \ln \{ \varepsilon_{11} \} = \frac{1}{\sqrt{3}} \ln \{ 1 + \gamma + \gamma^2/2 \} \quad (31)$$

The results for simple shear given in Fig. 5 are replotted in Fig. 7 against equivalent strain calculated using equations (5), (29) and (31). The use of equation (5) to calculate the equivalent strain when replotting the data for large strains is clearly not justified.

It is also evident that using equation (31) gives almost identical results to those for plane strain compression in Fig. 2. This is intuitively correct as both are plane strain deformation modes, but this conclusion conflicts with the result of Bate and Hutchinson⁹ that torsion is only half as effective as plane strain compression in increasing the grain boundary area. Overall it is concluded that equation (31) should be applied to the microstructural evolution in hot deformation, unless dynamic



7 Area ratio versus equivalent strains for cases illustrated

recrystallisation takes place to remove the distortion of the initial microstructure.

Hot working processes

The use of the appropriate relationships is important in modelling the effects of hot working by different industrial processes using the results from a variety of laboratory tests to discover the effects of initial grain size and strain on recrystallisation kinetics and recrystallised grain size. However, in applying the equations for S_V/S_{V_0} to multipass hot working conditions, it must be recognised that the strains involved are only those since the last cycle of recrystallisation, and that S_{V_0} is determined from the recrystallised grain size in equation (17). In practice, the non-uniform strain in grains will increase the value of S_V/S_{V_0} above that for uniform strain,⁹ but the irregularities in the grain boundaries that develop at subgrain boundaries are unlikely to be of concern, because the critical nucleus size for recrystallisation is larger than the mean subgrain size. Grain boundary sliding will reduce the value of S_V/S_{V_0} and become significant at low strain rates, e.g. in isothermal forging, and boundary sliding and grain growth become dominant in superplastic forming, when grains may not elongate. At very large strains, grain subdivision may become more significant than elongation of the original grains in increasing S_V/S_{V_0} . However, for normal industrial hot working conditions the computed values of S_V/S_{V_0} are considered to be appropriate for modelling recrystallisation behaviour.

Non-equiaxed grains

In practice, for example in many aluminium alloys, recrystallised grains may not be equiaxed, but have aspect ratios differing significantly from unity as a result of the prior thermomechanical processing conditions. In these cases, the number of grains per unit length N_{L1} , N_{L2} , and N_{L3} must be measured experimentally in the three orthogonal directions relevant to the subsequent thermomechanical processing operation. A nominal equiaxed linear intercept grain size for an equivalent grain of the same volume may be defined as

$$\bar{L}_{\text{nom}} = 1/N_{L(\text{average})} = (N_{L1}N_{L2}N_{L3})^{-1/3} \quad (32)$$

The grain shape can then be described in terms of apparent strains

$$\varepsilon_{i(\text{app})} = \ln\{N_{L_i}/N_{L(\text{ave})}\} \quad (33)$$

The effect of subsequent normal strain components can then simply be found, e.g. from equation (22), by replacing the applied strain components, ε_i by $\varepsilon_i + \varepsilon_{i(\text{app})}$. This simple analysis applies only when the axes of the elongated grain shape are the same as those of the subsequent deformation. It is also possible to have elongated grain structures that are not related to the deformation axes.

One example where the initial grain structure is highly elongated is the plate shape observed in martensitic microstructures. The method presented here is able to deal with this as long as the initial structure can be represented by a set of vectors.

Figures 8a and b show calculations for an initial microstructure of thin, square plates in which the thickness to long edge ratio is 0.05, typical of martensite. The dashed line represents a plate whose longest edges are oriented along [1 0 0] and [0 1 0] in the coordinate system of \mathcal{S} . The points as usual represent the 99 other randomly oriented plates, and the continuous line is the mean of this large set.

It is noticeable that the scatter is very large when compared with the tetrakaidecahedron, because the plate shape is so much more anisotropic that its orientation relative to the deformation becomes important. A comparison with Fig. 2 shows that the mean rates of creation of area and length with strain are similar, even though the maximum values are greater for plates.

Figure 8c shows the case for three specific orientations. Naturally, the change in area ratio is the greatest when the plane of the plate contains the rolling direction, and least when the plate thickness is parallel to the rolling direction.

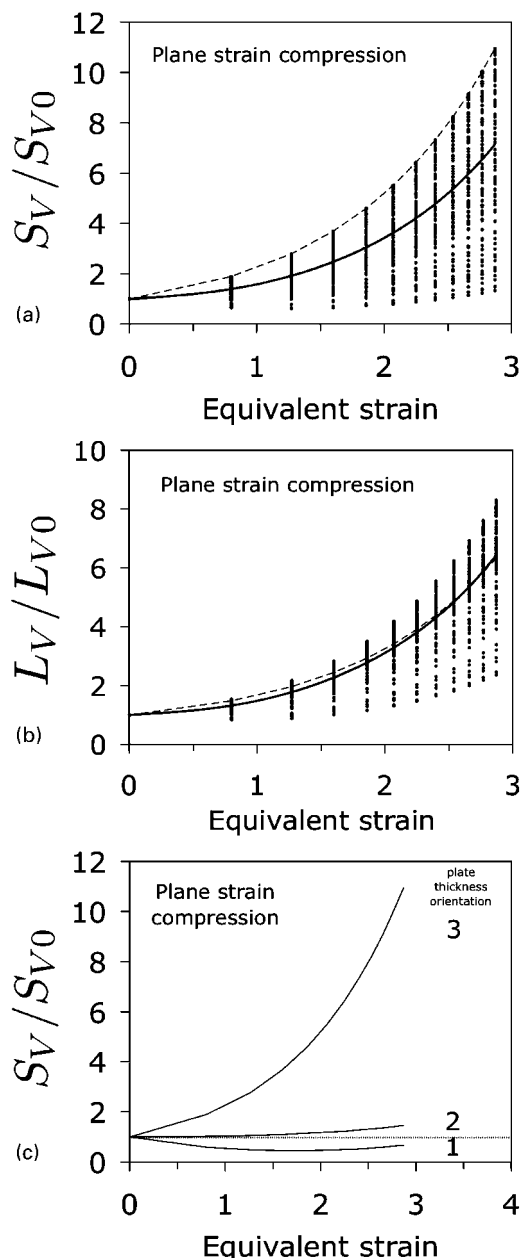
Sequential deformations

The effect of sequential deformations in different directions, as for example in the cross-rolling of plate, is illustrated in Fig. 9 which represents calculations done using equation (13). In this graph, the rolling strains are the same in both directions ($T_{11}=S_{11}$) and data for axisymmetric compression are also included (equations (8) and (9)). To allow a comparison between these deformation modes, the data are plotted as a function of the compressive strain. Notice that the axisymmetric compression and cross-rolling with equal strains in both directions give exactly identical results, illustrating that the results depend on the final strain components and not on the strain path to reach them.

The area ratio for single direction rolling is only slightly larger than for the cross-rolling when plotted against the compressive strain. This is not surprising given that for the same rolling reduction, the length along the rolling direction for single direction rolling will be much larger than obtained by cross-rolling. In contrast, the edge ratio becomes much larger for the single direction scenario, reflecting its greater microstructural anisotropy.

Complex deformations

Some results based on equation (14) for the combined effects of plane strain and simple shear deformation are illustrated in Fig. 10, where it is clear that the shear has



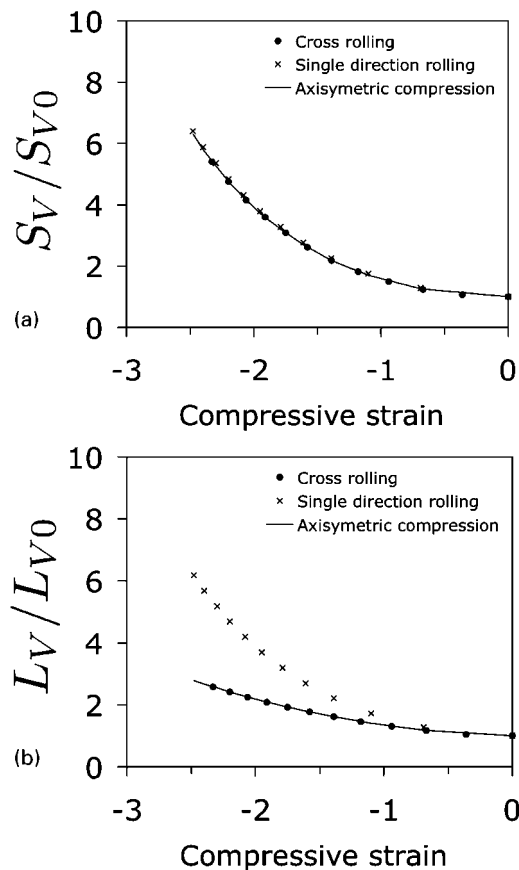
a area ratio versus equivalent strain; b edge ratio versus equivalent strain; c effect of plate orientation on area ratio

8 Calculations for plane strain compression for plate shaped objects: in image c, 1, 2 and 3 correspond to the rolling, invariant and compression directions respectively

a large effect on the description of the grain structures. Note that the shear strain in this combined mode is given by $S_{13} \times S_{11}$. The shear strain is maintained constant in each case by reducing S_{13} as S_{11} becomes larger. Under these conditions the effect of shear becomes negligible once ϵ_{11} becomes about unity. This is also the reason why the curves go through a minimum – as ϵ_{11} increases, S_{13} decreases in order to maintain a constant shear, thus eventually making the deformation matrix of equation (14) identical to that of plane strain compression.

Redundant shear strains in rolling

The redundant shears influence both the values of equivalent strain and of S_V/S_{V_0} at a given reduction in



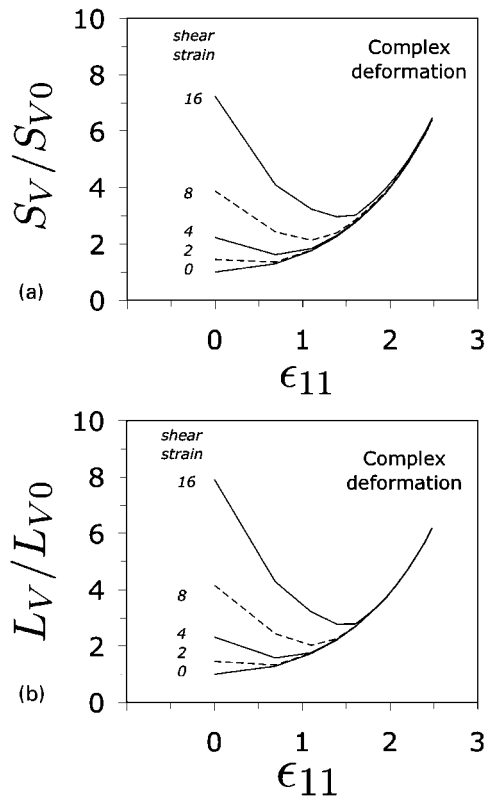
a area ratio versus compressive strain; b edge ratio versus compressive strain

9 Comparison of cross-rolling (identical strains in two rolling directions), axisymmetric compression and single direction rolling

thickness. Because the shear strain varies through the thickness, whereas for plane strain rolling the reduction in thickness, hence $\epsilon_{11} = -\epsilon_{33}$, is independent of position through the thickness, the results in this section are plotted against ϵ_{11} to avoid ambiguity. In Fig. 10 the effects of different constant (final) values of shear strain on boundary surface area and edge length are shown. It can be seen that as the grains become flattened by rolling the effect of a given final value of shear strain is reduced. In practice during rolling, the shear strain increases with increasing rolling reduction, with the result that the trajectories of S_V/S_{V_0} and L_V/L_{V_0} for any position in the thickness progressively cross the lines for higher constant final values of γ as shown in Fig. 10.

To achieve high total reductions, multipass rolling must be applied. If no recrystallisation takes place between passes, the shear strains of the grains increase progressively with reduction in forward–forward (tandem) rolling, but may be almost eliminated in forward–reverse rolling.¹⁹ In this context, it is important to recognise that the shear strain (shear angle) at the end of one pass is modified both by the reduction in thickness and by the shear in a subsequent pass. It is only the final net shear strain and reduction that are used to compute S_V/S_{V_0} and L_V/L_{V_0} .

As an example of through thickness effects, Fig. 11a shows the variation of shear strain through the thickness of an experimentally rolled slab given two forward passes of 50% reduction ($\epsilon_{11} = 1.386$, $\epsilon = 1.600$). The shear



a area ratio versus ϵ_{11} ; b edge ratio versus ϵ_{11}
 10 Calculations for combined plane strain deformation and simple shear (at strains illustrated), for tetrakaidcahedron oriented as illustrated in Fig. 1: shear strain is given by $S_{13} \times S_{11}$ in equation (14)

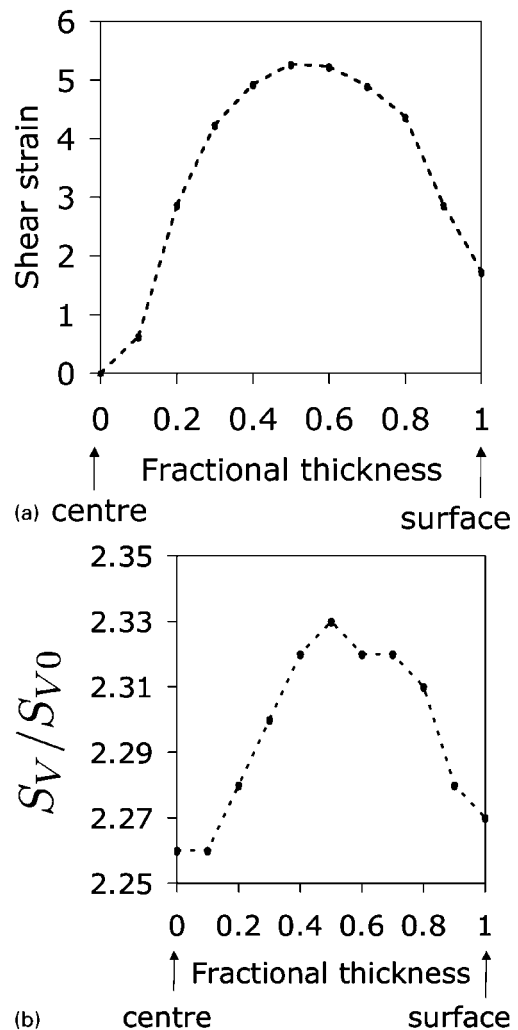
strains are computed from the distortions of finite element grids, which agree closely with the distortions of pins inserted through the thickness of the experimental slabs.¹⁹ Figure 11b shows the corresponding effect on S_V/S_{V_0} . It can be seen that the effect is relatively small compared with the effects of through thickness position on temperature, equivalent strain rate and strain, which determine the dislocation structure.

Grain size distributions

In the derivations using the deformation matrices, the austenite grains have always been assumed to be uniform in size. This is because it becomes simple to stack identical grains in three dimensions and fill all space. In practice there will always exist a distribution in the size of the grains. A possible method for dealing with such distributions is suggested here.

When experimental measurements of the grain size distribution are carried out, the data are presented without a consideration of the neighbourhoods of individual grains. In other words, it is known from the measurements that grains of a certain size have a certain frequency, but all information about their location is lost.

Therefore, it would be reasonable to consider the deformation of each size class separately. Suppose a volume fraction V_{V_i} is assigned to the i th size class. The changes in $(S_V/S_{V_0})_i$ and $(L_V/L_{V_0})_i$ can be calculated separately for that size class, and weighted with the volume fraction of that size class. The final values of



11 a measured variation in shear strain through thickness of rolled plate and b corresponding calculated variation in area ratio

these ratios are then given by

$$\frac{S_V}{S_{V_0}} \approx \frac{\sum_i V_{V_i} S_{V_i}}{\sum_i V_{V_i} S_{V_{0i}}} \quad \text{and} \quad \frac{L_V}{L_{V_0}} \approx \frac{\sum_i V_{V_i} L_{V_i}}{\sum_i V_{V_i} L_{V_{0i}}} \quad (34)$$

The approximation sign is necessary in this equation because in general, within a distribution of grain sizes, the grain shapes will not be identical. Furthermore, compatibilities of the deformations between different grain sizes have not been addressed.

Conclusions

Two quite different approaches to the quantitative metallography of deformed grains produce essentially identical results. The methodology in which a homogeneous deformation is applied to a particular shape is versatile in that equation (1) can in principle be applied to any grain shape or process, including others not covered in the present paper.

The software associated with all the calculations can be obtained freely from www.msm.cam.ac.uk/map/mapmain.html

References

1. E. E. Underwood: 'Quantitative stereology'; 1970, Reading, MA, Addison-Wesley Publication Company.

2. Y. van Leeuwen, S. Vooijs, J. Sietsma and S. Van der Zwaag: *Metall. Mater. Trans. A*, 1998, **29A**, 2925–2931.
3. I. Czinege and T. Reti: Proc. 18th Int. Machine Tool Design and Research Conf., London, England, September 1977, Imperial College, Vol. 1, 159–163.
4. S. B. Singh and H. K. D. H. Bhadeshia: *Mater. Sci. Technol.*, 1998, **15**, 832–834.
5. K. Matsuura and Y. Itoh: *Mater. Trans. JIM*, 1991, **32**, 1042–1047.
6. Y. Takayama, N. Furushiro, T. Tozawa, H. Kato and S. Hori: *Mater. Trans. JIM*, 1991, **32**, 214–221.
7. P. L. Orsetti Rossi and C. M. Sellars: *Acta Mater.*, 1997, **45**, 137–148.
8. M. Umemoto, H. Ohtsuka and I. Tamura: *Trans. ISIJ*, 1983, **23**, 775–784.
9. P. Bate and W. B. Hutchinson: *Scr. Mater.*, 2005, **52**, 199–203.
10. J. Gil-Sevillano, P. van Houtte and E. Aernoudt: *Prog. Mater. Sci.*, 1980, **27**, 69–314.
11. H. E. Vatne, T. Furu, R. Ørsund and E. Nes: *Acta Mater.*, 1996, **44**, 4463–4473.
12. O. Knustad, H. J. McQueen, N. Ryum and J. K. Solberg: *Practical Metallography*, 1985, **22**, 215.
13. H. K. D. H. Bhadeshia: 'Geometry of crystals', 2nd edn; 2001, London, Institute of Materials.
14. C. Mack: *Proc. Cambridge Philos. Soc.*, 1956, **52**, 286.
15. C. M. Sellars: Proc. Int. Conf. on 'Thermomechanical processing: theory, modelling and practice', (ed. B. Hutchinson *et al.*), 35–51; 1997, Stockholm, The Swedish Society for Materials Technology.
16. G. R. Canova, S. Chrivastava, J. J. Jonas and C. G'Sell: in 'Formability of metallic materials – 2000AD', (ed. J. R. Newby and B. A. Niemeir), ASTM STP 753, 1889–210; 1982, Philadelphia, PA, ASTM.
17. A. Nadai and E. Davis: *J. Appl. Phys.*, 1937, **8**, 205–217.
18. A. Eichinger: 'Werkstoffprüfung', Vol. 2, 715; 1955, Berlin, Springer-Verlag.
19. A. Mukhopadhyay, R. L. Higginson, I. C. Howard and C. M. Sellars: *Mater. Sci. Technol.*, 2007, **23**, 29–37.